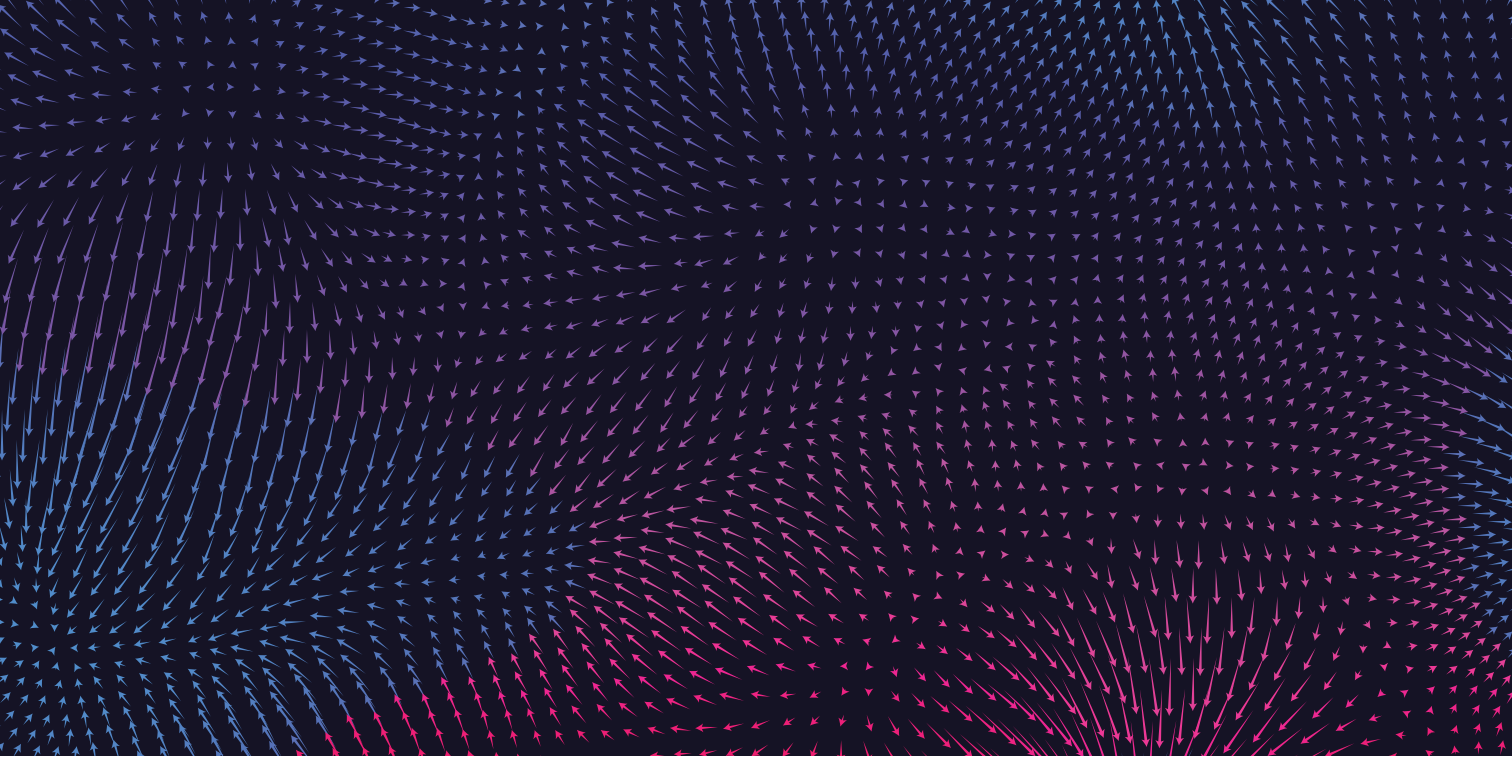

©SHUTTERSTOCK.COM/GARRYKILLIAN

Unveiling the Microworld Inside Magnetic Materials via Circuit Models

by Han (Helen) Cui, Saurav Dulal, Sadia Binte Sohid, Gong Gu, and Leon M. Tolbert

The progress made in wide bandgap (WBG) semiconductors has resulted in rapid miniaturization and increased efficiency of power converters. However, the improvements in magnetic components, such as inductors and transformers, have not kept pace with these advancements [1], [2], [3]. Although advances in WBG devices, novel

Digital Object Identifier 10.1109/MPEL.2023.3301408
Date of publication: 26 September 2023

2329-9207/23©2023IEEE

topologies, control schemes, and hardware fabrications have greatly improved circuit efficiency and power density, the bottleneck now lies with magnetic components [4], with magnetics accounting for more than 30% of the cost and more than 30% of the loss in almost all power converters [5]. Magnetics design has become a critical issue for power electronics as trends towards high efficiency and high power-density.

The limits set by bulky and lossy magnetic components must be broken by 1) radically new magnetic design techniques and 2) novel magnetic materials with improved properties (e.g., higher saturation limit, higher permeability, and lower core loss).

Why is it Difficult to Deal With Magnetics?

The challenges of magnetics design and optimization are attributed to two main aspects, both of which must be addressed by magnetic material modeling capable of predicting component behaviors:

First, deep understanding and accurate design tools are required in magnetic components to comply with the trend towards high frequency and high density. Instead of being satisfied with the performance given by an off-the-shelf inductor, power electronics engineers nowadays are obliged to design magnetic components from scratch with highly customized cores and windings that yield better performance. This requires advanced knowledge of magnetic materials, loss analysis, high-frequency effects, and simulations that aid the design. Advanced electromagnetic simulators [6], such as 3D finite-element analysis (FEA) tools, are able to simulate linear performance factors governed by the Maxwell's equations, including winding loss, fringing effect, geometry-based non-uniformity, and even numerical optimizations. However, there is one exception, and it is the major one that causes the discrepancies seen frequently between simulations and real prototypes: the nonlinear magnetic materials. Lack of accurate models and understanding of the material's properties (such as dc bias- and frequency-dependent loss and permeability) when used as a power electronics component results in oversimplified assumptions in magnetic design and then iterations of magnetics prototyping based on trial and error.

Second, new magnetic materials are needed to break the ceiling of magnetic component performance set by intrinsic physical properties (e.g., saturation level, permeability, and loss density) of existing materials. To this end, component or even system level insights are essential to guide new materials development. However, magnetic components design is not a single-objective optimization process [7]; an optimal design balances several performance factors. For example, a material that has an infinitely large permeability, but low saturation level, doesn't necessarily lead to improved component performance. An envisioned paradigm of material-component-system co-design needs to be facilitated by a simulation platform that links magnetic material properties component prototype performance metrics.

However, magnetic materials modeling is never an easy job. The two most concerned performances of magnetic materials in power electronics applications are permeability and core loss, both of which vary significantly with frequency and the strength of the magnetic field (excitation signal) applied. Take the MnZn ferrite material N87 from TDK [8] as an example (Figure 1). The nonlinear permeability and core loss vary with frequency and ac excitation amplitude. Besides the nonlinearity with ac excitation, the effect of dc bias on the permeability and loss also strongly impacts the core performance [9]. Such complexities, rooted in the nonlinear dynamics of magnetic materials, hinder good agreement between designs and prototypes of magnetic components and lead to multiple trial and error in engineering practice.

In practice, power electronics engineers tend to use empirical approaches to characterize magnetic materials based on large-signal measurements. Models to account for the core loss and permeability, mostly empirical, are extracted by curve-fitting experimental results measured from specific prototypes [10], [11], with measurements getting more extensive as more complex behaviors of the core are observed. Even the physics-based models

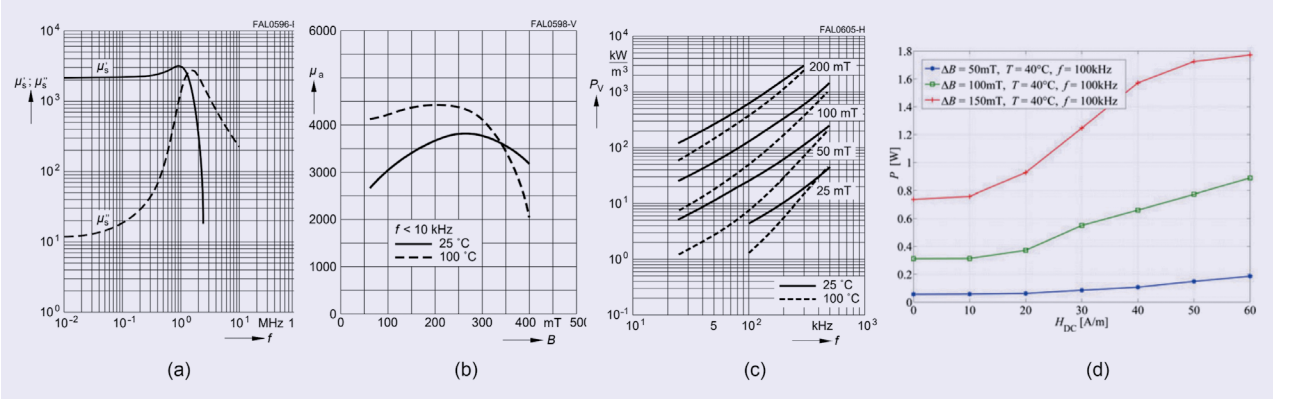

FIG 1 Nonlinear behaviors of magnetic material N87: (a) permeability versus frequency, (b) permeability versus ac excitation amplitude, (c) core loss density versus frequency and ac excitation amplitude [7], and (d) core loss versus dc bias [8].

do not capture the nonlinear dynamics properly, as none of the model accounts for all aspects of the complicated physics. Prominent examples include the Jiles–Atherton (J–A) [12] and Preisach models [13]: The former attributes magnetic hysteresis to a single frictional mechanism—domain wall movement impeded by defect pinning, and the latter is based on the Stoner–Wohlfarth theory that concerns only the energy minimization with no regards by itself to the dynamics of the material system. Nowadays, assisted by powerful artificial intelligence (AI) tools, researchers are able to conduct large-scale measurements and model extractions to get more accurate performance predictions [14], [15]. However, the biggest issue with AI models is that they are only as good as the data they are trained on and provide no insights on how they arrived at their results.

More desirable for the next-generation power electronics is a bottom-up solution (Figure 2), based on the physics underlying the behavior of magnetic materials in components, thus allowing for component behavior prediction in a wide range of operating conditions to enable design optimization. Moreover, physics-based magnetics modeling on the material level bridges the gap between the material science and power electronics communities by providing a common platform, on which the problems related to magnetization and loss mechanisms can be better framed, thus fostering innovations in magnetic materials research for power electronics. Nevertheless, the computational cost of physics-based magnetic material modeling can be prohibitively high, therefore trade-offs must be made at the onset. Fortunately, a mesoscopic view [16] provides appropriate trade-offs that enable, in principle, predictive modeling at reasonable cost: while the atomic-scale origin of ferromagnetism, the exchange interaction between electron magnetic moments, is quantum in nature without a classical analog, a magnet is treated as a mesoscopic continuous medium described by magnetization $\boldsymbol{M}(\boldsymbol{r})$ as a continuously varying function of location $\boldsymbol{r}$. The mesoscopically continuous medium is discretized into regions each described by local magnetization $\boldsymbol{M}$, following time-domain differential equations describing their dynamics and coupling with neighboring regions. Such a region is sufficiently large on the atomic scale for quantum effects to average out, thus the differential equation is a classical, albeit nonlinear, one. The course graining and the relatively simple classical equation at the bottom level will enable this approach to capture the nonlinear dynamics at adequate accuracies at practically acceptable computational costs.

This article describes a novel implementation of such a bottom-up solution. The nonlinear differential equation of a discretized region is mapped to a mathematically equivalent circuit model such that the collective dynamic response of the coupled regions to external field excitations is emulated by that of the coupled unit circuits to circuit excitations. Thus, the simulations will be performed using circuit simulators that power electronic engineers are already familiar with. Preliminary results are reported on some simplified cases to show the potential of such models in describing the nonlinear B–H hysteresis and loss behaviors. Use cases are presented to demonstrate the capability of the model for magnetics used in both power electronics and microwave applications. The model will be augmented and scaled up to include more physical mechanisms.

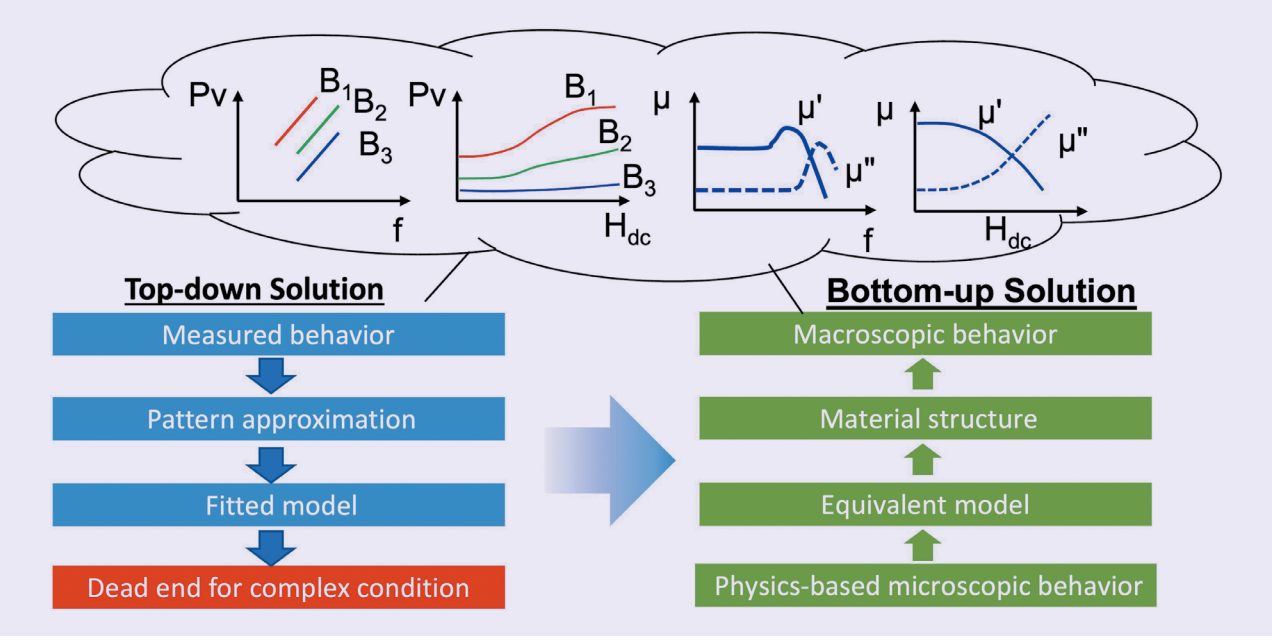

FIG 2 In contrast to the conventional "top-down" solution for magnetics modeling, we propose to develop a novel "bottom-up" solution.

Physics Based Circuit Models for Magnetic Materials

Every performance metric of a magnetic component originates from the response of its core material to external field excitations; the core is a soft magnet. Ferromagnetism originates from the magnetic moment of the electron spin. Strong but short-range exchange interaction aligns the electron spins within a distance in the order of 10 nm, but long-range interactions favor a random distribution of magnetization, which is the total magnetic moment per volume. The balance results in the formation of magnetic domains, each a region of uniform magnetization (Figure 3). The dynamics of a magnetic material boils down to the time evolution of the domains, which is described by the Landau–Lifshitz–Gilbert (LLG) equation.

LLG Equation

The LLG equation [16] describes the dynamics of magnetization $\boldsymbol{M}$, presumed uniform throughout a magnetic material sample or a region therein:

$$\frac{d\boldsymbol{M}}{dt} = -\mu_0\gamma \boldsymbol{M}\times\boldsymbol{H}_{\text{eff}} + \frac{\alpha}{\boldsymbol{M}_s}\boldsymbol{M}\times\frac{d\boldsymbol{M}}{dt} \tag{1}$$

where the vacuum permeability μ_0 is a physical constant. Here, we emphasize that $\boldsymbol{H}_{\text{eff}} = \boldsymbol{H} + \boldsymbol{H}_e$ is the total effective field including the magnetic field $\boldsymbol{H}$ and the effective field $\boldsymbol{H}_e$, which is the sum of effective fields that represent the material anisotropy, exchange interaction, etc. Without the second term on the right side, (1) is in the same form as the dynamics of an *isolated* electron magnetic moment $d\boldsymbol{m}/dt = -\mu_0\gamma\boldsymbol{m}\times\boldsymbol{H}$, where there is no distinction between $\boldsymbol{H}_{\text{eff}}$ and $\boldsymbol{H}$, and $\gamma = 1.759\times10^{11}$ C/kg is the electron charge-to-mass ratio, which is identical to the ratio of the moment to spin angular momentum, named the gyromagnetic ratio. This equation simply describes the precession of the electron spin angular momentum and, proportionally, $\boldsymbol{m}$, driven by the torque exerted by $\boldsymbol{H}_{\text{eff}}$. The isolated electron spin precesses indefinitely because the torque is always perpendicular to $\boldsymbol{m}$. Since ferromagnetism arises from electron spins, we can replace $\boldsymbol{m}$ with $\boldsymbol{M}$, i.e., the sum of magnetic moments of all N electrons contributing to ferromagnetism in a unit volume of a material. Due to other effects in the material, however, the precession is damped, and therefore $\boldsymbol{M}$ gradually aligns with $\boldsymbol{H}_{\text{eff}}$ in what is referred to as the magnetization process. To describe this lossy process, the second term is phenomenologically introduced to (1), where α is the damping parameter and $M_s = Nm = |\boldsymbol{M}|$ is the saturation magnetization; both parameters are to be obtained from standard material characterization. Lastly, γ is slightly modified from the isolated electron value to account for atomic structures of specific materials.

Equation (1) is written as three coupled differential equations in three Cartesian projections. Examining these equations, we see that they are formally the same as the set of equations describing a circuit of coupled elements: Each of the three equations, written in a form with all terms on one side and zero on the other, resembles Kirchoff's current law (KCL) upon mapping M_i, $i = x$, y, z, to linkages Λ_i of three coupled inductors L_i, and H_z to excitation current I_z; L_i are considered wound around a shared core just share the same flux. The mapping leads us to an equivalent circuit model shown in Figure 4 (more details below), where the three ports correspond to the three Cartesian projections, with the voltages $V_i = d\Lambda_i/dt$ surrogating dM_i/dt.

To illustrate our bottom-up modeling framework, let us start with a fictitious single-domain inductor core Δz long with a $\Delta x\times\Delta y$ rectangular cross section. Assuming an isotropic core material and neglecting the demagnetizing field for now, we have $\boldsymbol{H}_{\text{eff}} = \boldsymbol{H} = H_z\hat{\boldsymbol{z}}$, where $H_z = I_z/\Delta z$ is due to the only excitation—current through the inductor

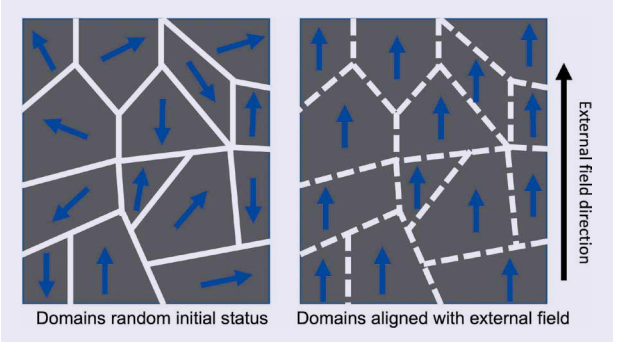

FIG 3 Illustration of magnetic domains of a soft magnetic material lining up when exposed to an external magnetic field.

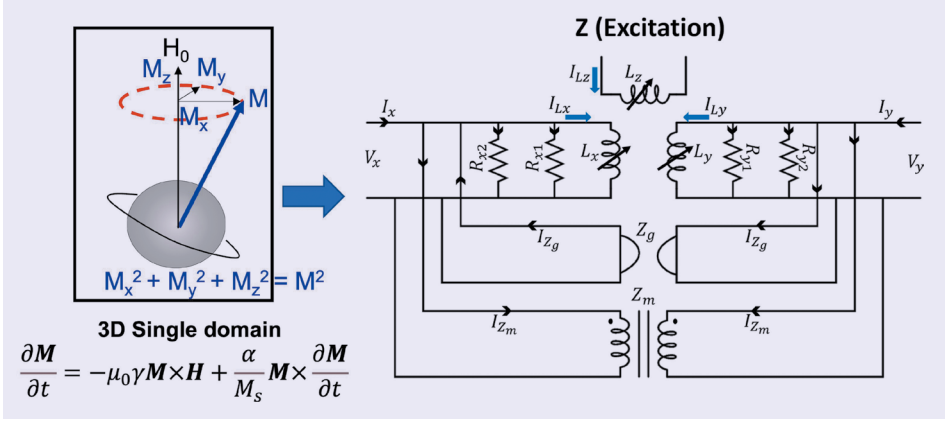

FIG 4 Equivalent circuit with parameters derived from the full LLG equation describing a magnetic domain's movement in 3D *x*–*y*–*z* planes with external excitation field applied on the *z* direction.

winding (per Ampere's law). Proportional constants in the above mapping of dM_i/dt and H_z to surrogate voltages V_i and currents I_z can be chosen arbitrarily. Interestingly, by choosing mapping proportions such that $H_z \to I_z = H_z\Delta z$ and $dM_z/dt \to V_z = \mu_0\Delta x\Delta y(dM_z/dt)$, the current I_z and voltage V_z in the equivalent circuit coincide with the current and the voltage per turn of the *physical* inductor (approximately for voltage given relative permeability $\mu_r \gg 1$), allowing for direct integration of material modeling into a circuit simulator to simulate a physical circuit. The mapping of quantities in all three dimensions to the surrogate circuit quantities is as follows:

$$\begin{aligned} V_x &= \mu_0\Delta y\Delta z\frac{dM_x}{dt}, V_y = \mu_0\Delta x\Delta z\frac{dM_y}{dt}, \\ V_z &= \mu_0\Delta y\Delta x\frac{dM_z}{dt}, I_z = H_z\cdot\Delta z. \end{aligned} \tag{2}$$

Substituting the circuit surrogates defined by (2) into the three differential equations re-written from (1) and then eliminating dM_z/dt using the z-projection equation, the two remaining equations for x and y projections become:

$$\begin{aligned} 0 = &\frac{V_x}{\mu_0^2\gamma M_z\Delta z} + \frac{\Delta y H_z\cdot\int V_y dt}{\mu_0\Delta x\Delta z M_z} + \frac{\alpha\Delta y\cdot V_y}{\mu_0^2\gamma M_s\Delta x\Delta z} \\ &+ \frac{\alpha M_x M_y\cdot V_x}{\mu_0^2\gamma M_s M_z^2\Delta z} + \frac{\alpha M_y^2\Delta y\cdot V_y}{\mu_0^2\gamma M_s M_z^2\Delta x\Delta z} \end{aligned} \tag{3}$$

$$\begin{aligned} 0 = &-\frac{V_y}{\mu_0^2\gamma M_z\Delta z} + \frac{\Delta x H_z\cdot\int V_x dt}{\mu_0\Delta y\Delta z M_z} \\ &+ \frac{\alpha\Delta x\cdot V_x}{\mu_0^2\gamma M_s\Delta y\Delta z} + \frac{\alpha M_x M_y\cdot V_y}{\mu_0^2\gamma M_s M_z^2\Delta z} + \frac{\alpha M_x^2\Delta x\cdot V_x}{\mu_0^2\gamma M_s M_z^2\Delta y\Delta z}. \end{aligned} \tag{4}$$

Equivalent Circuit for LLG Equation

Equations (3) and (4) are actually KCL equations at ports x and y of the three-port circuit when the excitation is applied only to port z. The total currents at ports x and y each consist of five components that add up to zero, expressed as follows in terms of the equivalent circuit elements labeled in Figure 4:

$$0 = \frac{V_x}{Z_g} + \frac{\int V_y dt}{L_y} + \frac{V_y}{R_{y1}} + \frac{V_x}{Z_m} + \frac{V_y}{R_{y2}} \tag{5}$$

$$0 = -\frac{V_y}{Z_g} + \frac{\int V_x dt}{L_x} + \frac{V_x}{R_{x1}} + \frac{V_y}{Z_m} + \frac{V_x}{R_{x2}}. \tag{6}$$

The inductors L_x and L_y with coupling to the z port is thus determined to be

$$L_y = \frac{\mu_0\Delta x\Delta z M_z}{\Delta y H_z}, \qquad L_x = \frac{\mu_0\Delta y\Delta z M_z}{\Delta x H_z}, \tag{7}$$

along with additional elements: R_{x1} and R_{y1} are linear resistors, while R_{x2} and R_{y2} are nonlinear resistors across port x and y, respectively, given by

$$\begin{aligned} R_{x1} &= \frac{\mu_0^2\gamma M_s\Delta y\Delta z}{\alpha\Delta x}, R_{y1} = \frac{\mu_0^2\gamma M_s\Delta x\Delta z}{\alpha\Delta y}, \\ R_{x2} &= \frac{\mu_0^2\gamma M_s M_z^2\Delta y\Delta z}{\alpha M_x^2\Delta x}, R_{y2} = \frac{\mu_0^2\gamma M_s M_z^2\Delta x\Delta z}{\alpha M_y^2\Delta y}; \end{aligned} \tag{8}$$

a gyrator with impedance Z_g and a 1:1 transformer with all equal self and mutual impedances Z_m couple ports x and y:

$$Z_g = \mu_0^2\gamma M_z\Delta z, \qquad Z_m = \frac{\mu_0^2\gamma M_s M_z^2\Delta z}{\alpha M_x M_y}. \tag{9}$$

Notice that definitions of V_z and I_z in (2) directly result in $L_z = d\Lambda_z/dt = (\mu_0\Delta x\Delta y M_z)/(\Delta x H_z)$, which, along with (7), indicate that the three coupled inductor share the same flux ϕ that can be mapped to M_z.

Modeling Results

The equivalent circuit in Figure 4 can be constructed in any circuit simulator that allows user-defined terminal functions. The circuit requires one input at one port (z in the example) representing the winding current, the dimension of the single-domain core (i.e., Δx, Δy, and Δz), and two material properties α and M_s, both of which can be experimentally determined by measuring the frequency-dependent magnetic susceptibility of the material. The outputs of the model are the voltages and currents on each of the three terminals (V_x, V_y, V_z, I_x, I_y, I_z), which correspond to the magnetization and magnetic field along each direction as suggested by (2). By varying the excitation signal applied to the input side, the output can be measured in voltage and examined dynamically in time-domain that reflects what happens inside the microworld of the magnetic material. This serves as a valuable tool to transparently connect the material's properties to its function and performance in a power electronics system in the language of circuits.

Nonlinear Magnetization Process

As a preliminary test run of the model, a fictitious single domain with a size of 200 μm × 50 μm × 38 mm, damping constant of 5×10^{-4}, and magnetization of 1750 Oe was used. An external dc magnetic field was applied to the domain in terms of a current source. The magnitude of the dc field was increased from 0 to 100 Oe in the z direction, and the domain was assumed to be aligned originally along the x direction by defining the initial conditions of the voltages on the three terminals. The magnetization process happens when the domain starts to rotate and gets aligned with the external field and eventually gets saturated, which can all be observed vividly from the waveforms of M_x, M_y, and M_z translated from the V_x, V_y, and V_z. As shown in Figure 5, this process is plotted in 3D showing the trajectory of the domain magnetization process from the initial state of alignment with x (M_x = 1750 Oe) that then slowly spirals to the final state of saturation along the z direction (M_z = 1750 Oe).

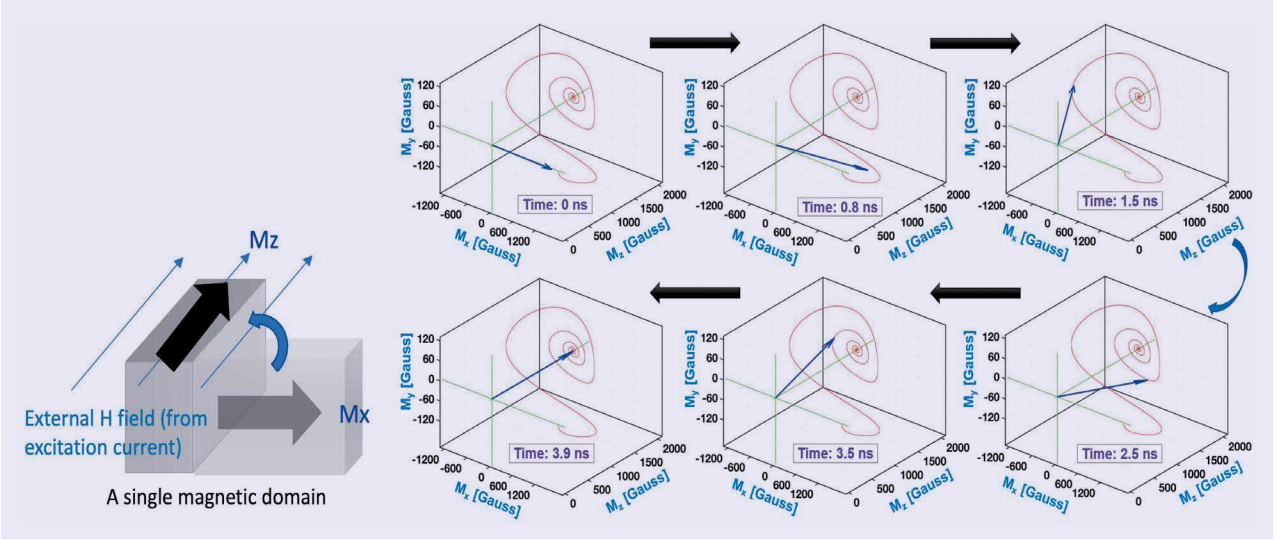

FIG 5 Time lapse and trajectory of a magnetic domain rotation starting with aligned on the *x* direction and gradually rotates to the *z* direction on which the external field is applied.

The complete 3D modeling of the domain rotation, rather than 1D or 2D, preserves the full picture of how the domain moves, providing interconnecting capability to simulate 3D couplings with multiple domains.

To further showcase the capability of the model, we show that a hysteresis loop can be simulated (results shown in Figure 6) by simply introducing an anisotropy field $\boldsymbol{H}_{\text{ani}}$, and that nonlinear M–H curve and nonlinear permeability can be readily extracted from simulation results. A constant anisotropy field is introduced by adding constant current sources to the ports to simulate magnetocrystalline anisotropy that tilts the easy axis away from $\hat{\boldsymbol{z}}$. As the external excitation field H_z increases in time, $\boldsymbol{M}$ spirals towards the direction of $\boldsymbol{H}_{\text{eff}} = H_z\hat{\boldsymbol{z}} + \boldsymbol{H}_{\text{ani}}$ and thus M_z increases. The susceptibility is extracted by $\chi = M_z/H_z$, and the relative permeability is simply $\mu_r = 1 + \chi$, shown in Figure 6(a) as extracted along the curve as H_z drops to zero after the saturation. As the external field decreases and reverses, $\boldsymbol{M}$ moves away from the $\hat{\boldsymbol{z}}$ direction as it precesses around the total effective field, giving rise to hysteresis. By reversing the external field twice, the full hysteresis loop is captured, as shown in Figure 6(b). These results demonstrate for the first time that the micro-dynamics in magnetic materials can be represented and simulated in circuit solvers, which directly links a magnetic material parameter to power electronics component behavior.

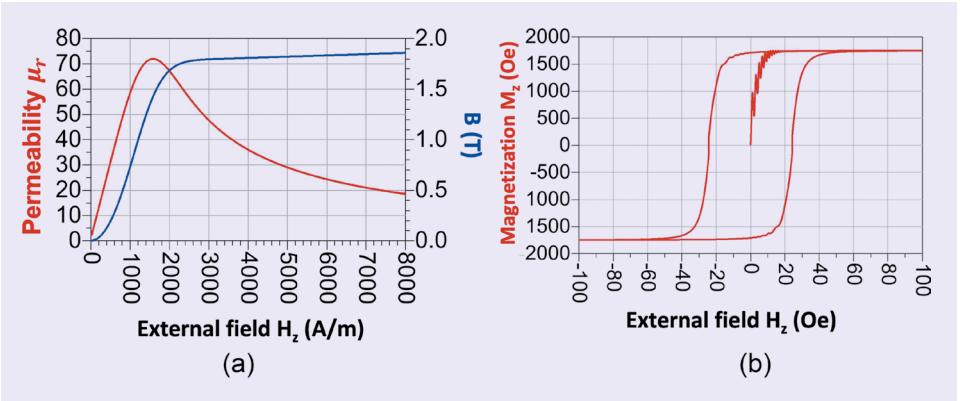

FIG 6 Simulation results from the circuit model of a magnetic domain under an external magnetic field *H* along the *z* direction showing (a) nonlinear permeability and flux density *B* versus external field *H* and (b) initial magnetization curve and hysteresis loop.

The LLG-based model has long been used in microwave applications [16], and was more recently implemented with equivalent circuits. Compared to power electronics applications, microwave applications have a simpler scenario to address, where a strong dc field in one direction biases all domains near saturation thus the high-frequency field driving $\boldsymbol{M}$ to precess at a small angle can be treated as a small signal. Therefore, the nonlinear resistors R_{x2} and R_{y2} as well as the 1:1 transformer Z_m in Figure 4 can be ignored. As an example, the frequency-selective limiter (FSL) is a waveguide loaded with a piece of magnetic material that utilizes the nonlinear insertion loss in magnetics to attenuate input signals at different amplitudes [17]. The circuit model has been proven effective to predict the nonlinear losses and time delays for the filtering performance as demonstrated in [17] and [18].

Scaling up to Bulk Materials and Refining the Model

The above examples showcase the potential of the proposed modeling framework, in simple cases where the core can be treated as having a uniform $\boldsymbol{M}$. In the discussion of scaling up, we refer to a region of uniform $\boldsymbol{M}$ governed by (1) in a core material as a "domain," which does not necessarily identify with a physical magnetic domain although conceptually similar. We first point out that a single-domain model can already simulate some special cases. A demagnetization field $\boldsymbol{H}_d$ dependent on $\boldsymbol{M}$ can be added to simulate the shape anisotropy of a long, thin core made of a soft magnetic material, because the long-range interaction is embedded in the $\boldsymbol{M}$ dependence in $\boldsymbol{H}_d$. This can be implemented by utilizing ports x and y in Figure 4. At the relatively low frequencies of interest to power electronics (even for fast-switching converters enabled by future magnetic materials), the effect of initial $\boldsymbol{M}$ orientations is insignificant therefore the single-domain model is expected to achieve adequate accuracy. This model will work even better for a thin torus, with the cross section area and axial perimeter substituting $\Delta x\Delta y$ and Δz, respectively. Other core shapes can be simulated by using the appropriate $\boldsymbol{H}_d$ versus $\boldsymbol{M}$ dependence in accordance with the demagnetizing tensors. Furthermore, a magnetocrystalline anisotropy field $\boldsymbol{H}_{\text{ani}}$ can be added as exemplified above (Figure 6), with an orientation determined by the fabrication process. Worth pointing out is the flexibility afforded by the LLG equation in accommodating various physics through various effective fields. We mention in passing that $\boldsymbol{H}_d$, while acting similarly, is conceptually not an effective field, but rather a part of $\boldsymbol{H}$, which is determined by the winding current per Ampere's law.

Multiple domains will be needed in general. For example, the easy and hard axes may be oriented in different directions with regard to the core geometry, requiring different $\boldsymbol{H}_{\text{ani}}$ in different regions. In a multi-domain model, each domain n is represented by a three-port circuit simulating the dynamics of its magnetization $\boldsymbol{M}_n$, and the susceptibility is extracted by $\chi = [\sum_n (\hat{\boldsymbol{z}} \cdot \boldsymbol{M}_n \Delta V_n)/V]/H_z$, where ΔV_n and V are the volume of domain n and the total volume, respectively. We expect the use of "domains" larger than physical magnetic domains to lower the computational cost in most cases, as in a previous LLG-based model [19], where the $(0.1\ \text{mm})^3$ discretized region is already much larger than typical physical domains while only a $16 \times 16 \times 8$ array of such regions was modeled to represent a magnetic core orders of magnitude larger in volume.

The on-going efforts of this work involve adding physical mechanisms for the model to be adequate in more and more application scenarios to predict core loss and nonlinear permeability with a small number of physically meaningful and measurable parameters, in contrast to the extensive curve fitting as currently practiced. Down the road, neighboring domain interactions will be incorporated as coupling circuit elements to account for domain wall motion under exchange interactions within a single-crystal material, a crystal grain of polycrystalline materials, or an amorphous material. Finally, the domain wall motion impeding effects of grain boundaries, as visualized in cartoon illustration (Figure 7c), as well as other defects, will be captured. This framework is versatile to accommodate various physical mechanisms through effective fields, thanks to the flexibility of the single-domain circuit (Figure 4): while the excitation is applied only to port z, ports x and y can be connected to current sources representing effective fields. Separately on the single-domain level, the stochastic process of thermal relaxation may need to be incorporated. Overall, the parameters of the circuit model will be physical properties that can be extracted from material characterizations such as saturation flux density, ferromagnetic resonance quality factor, etc. The loss and permeability of the magnetic core can be simulated and extracted as the real and imaginary parts of the input impedance seen by the excitation source in the circuit model. By fine-tuning the model parameters, the loss and permeability should match bulk material and component measurement results. This model calibration is fundamentally different from empirical curve fitting, in that our model parameters bear physical meanings. Therefore, the accuracy gained by model calibration will be transferrable to components based on the same material but of different geometries and under different operation conditions,

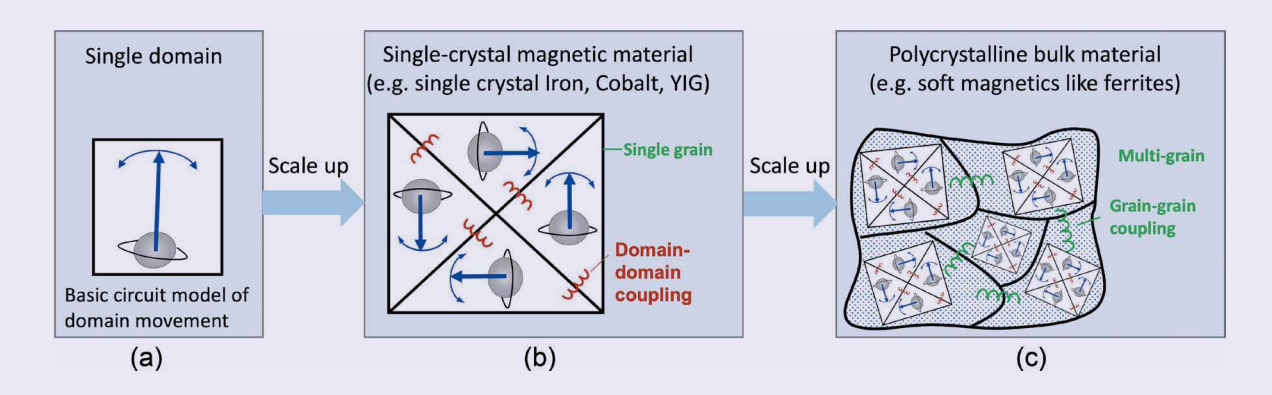

FIG 7 Illustration of the scale-up process from the circuit model of (a) single magnetic domain to (b) single-crystal materials and (c) polycrystal magnetic materials.

the frequency- and amplitude-dependency in the magnetic material properties result naturally from the dynamics described by the LLG.

How Artifical Intelligence (AI) Can Help With Physics-Based Models?

Physics-based models are powerful tools to predict and understand the root cause of magnetic material behaviors. However, they will reach a limit when practical issues such as material impurities or irregular microstructures are taken into account. This is the general issue with bottom-up solutions where scaling-up is the most challenging part. On the other hand, typical top-down solutions such as AI-based or machine-learning methods are being developed, typically with limited physical insights. Therefore, it would be ideal that AI and physics-based models could work together in a complementary manner to enhance the accuracy and efficiency of modeling magnetic materials. The following are two possible ways:

1) *Data-Driven Modeling on Non-Ideal Physical Factors:* AI algorithms can be trained on large datasets of experimental or simulated data. By analyzing the data, AI models can identify patterns and relationships that may be difficult to detect using traditional physics-based modeling techniques such as complex microstructures in the material. These data-driven models for equivalent microstructures can then be integrated with physics-based models to assist the scaling-up and improve the predictive power.
2) *Optimization and Design Process:* AI algorithms can be used in conjunction with physics-based models to optimize the design of magnetics for specific applications. For example, AI models can be used to identify the optimal parameters for the circuit models that can enhance the entire performance of a power electronics system, such as the optimal shape of a magnetic component or the optimal material's structure.

Overall, the integration of AI and physics-based models will help in developing more accurate, efficient, and comprehensive models for the complex behaviors in magnetic materials and facilitate the WBG applications. By leveraging the strengths of both approaches, the goal is to develop a physics-informed intelligent model that bridges the gap between material science and power electronics as illustrated in Figure 8. By integrating the two areas, system-level inputs on the component specification can be provided to guide the material development, while the physics-based model will facilitate the identification of new material and their properties predictions.

Conclusion

Equivalent circuit modeling is expected to be an effective way to connect the material's properties with their component behaviors in the power electronics systems. This article discusses a circuit model derived from the equation of motion for magnetic domains that concisely represents and illustrates material dynamic physics. The objective is to provide a new layer of foundation to explain the nonlinear complex behaviors in magnetic core losses and permeabilities. Single magnetic domain dynamics has been simulated, which serves as the basis for the hierarchical scaling that entails the incorporation of more physical mechanisms as couplings among the single-domain circuits. The circuit model can be integrated with system level simulations where the magnetic component is used, thereby providing a path penetrating the material properties and the circuit applications. As power electronics continue to advance, it becomes increasingly important to delve deeper into the underlying principles and behavior of these systems through fundamental research. By doing so, a more comprehensive

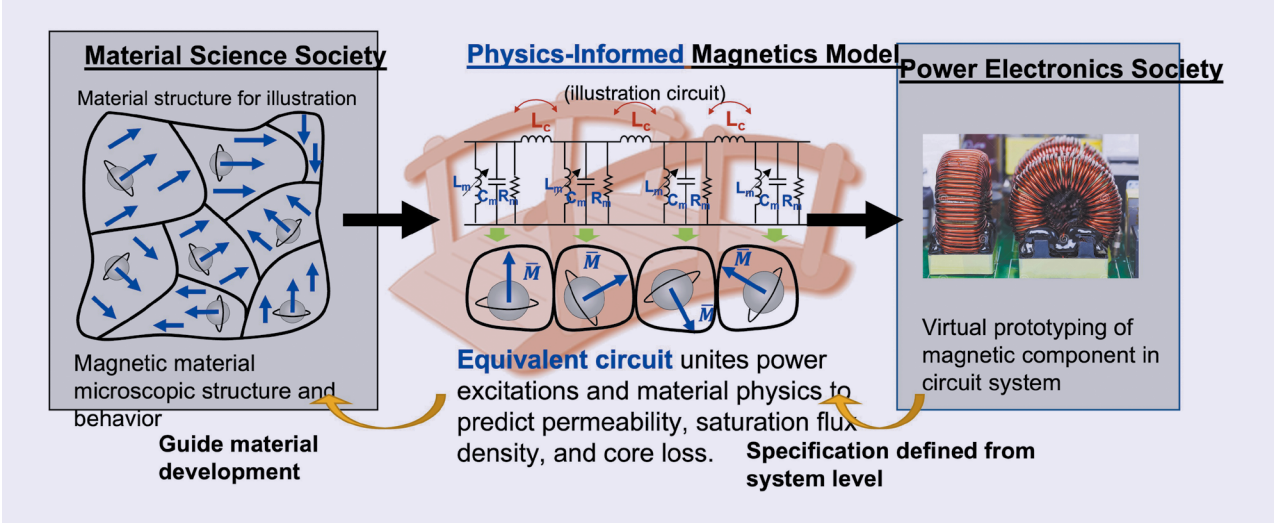

FIG 8 Equivalent circuit modeling scheme connecting material-level structure and component-level performance without need of trial-and-error prototype measurements; it also provides guidelines on material microstructure to expedite the material development and optimization process.

understanding can be gained of the complexities involved and identify new avenues for innovation and advancement, enabling us to push the boundaries of what is possible and achieve new levels of performance and efficiency in power electronics.

Acknowledgment

This work was supported by the Office of Naval Research under Grant Award N00014-22-1-2545 titled "A multiscale physic-based magnetics design framework for ship scale power electronics."

About the Authors

Han (Helen) Cui (helencui@utk.edu) received the B.S. degree in electrical engineering from Tianjin University, Tianjin, China, in 2011, and the M.S. and Ph.D. degrees in electrical engineering from Virginia Tech, Blacksburg, VA, USA, in 2013 and 2017, respectively. Upon graduation, she joined the Electrical and Computer Engineering Department, University of California, Los Angeles, CA, USA, as a Post-Doctoral Researcher to expand the knowledge of magnetics modeling for high-frequency RF applications. She has been an Assistant Professor with the University of Tennessee, Knoxville, TN, USA, since 2020. Her research interests include magnetic designs and integration for WBG device applications, advanced power electronics packaging, electromagnetic devices for sensing, and microscopic magnetics.

Saurav Dulal received the bachelor's degree in electrical engineering from Pulchowk Campus, Tribhuvan University, Nepal, in 2021. He is currently pursuing the Ph.D. degree with the Department of Electrical Engineering and Computer Science, The University of Tennessee, Knoxville, TN, USA. His research interests include magnetic modeling, modeling of power converters, and application of power electronics in electric vehicles.

Sadia Binte Sohid received the B.S. degree in electrical and electronic engineering from the Rajshahi University of Engineering and Technology, Rajshahi, Bangladesh, in 2015, and the M.S. degree in electrical engineering from Bucknell University, Lewisburg, PA, USA, in 2019. She is currently pursuing the Ph.D. degree in electrical engineering with the University of Tennessee, Knoxville, TN, USA. Her research interests include power electronics and magnetic design.

Gong Gu is a Professor of electrical engineering with the University of Tennessee, Knoxville, TN, USA. His research interests are in novel materials for electronic device applications. He received the Ph.D. degree from Princeton University, Princeton, NJ, USA, and the bachelor's degree from Tsinghua University, Beijing, China.

Leon M. Tolbert received the bachelor's, M.S., and Ph.D. degrees in electrical engineering from the Georgia Institute of Technology, Atlanta, GA, USA. He is currently the Chancellor's Professor and the Min H. Kao Professor with the Department of Electrical Engineering and Computer Science, The University of Tennessee, Knoxville, TN, USA. He is also an Adjunct Participant with Oak Ridge National Laboratory, where he previously worked from 1991 to 2020. His research interests include electric vehicles, application of wide bandgap semiconductors, and the utility application of power electronics for renewable energy and energy storage.

References

[1] J. M. Silveyra et al., "Soft magnetic materials for a sustainable and electrified world," *Science*, vol. 362, no. 6413, Oct. 2018, Art. no. eaao0195.

[2] F. C. Lee, Q. Li, and A. Nabih, "High frequency resonant converters: An overview on the magnetic design and control methods," *IEEE J. Emerg. Sel. Topics Power Electron.*, vol. 9, no. 1, pp. 11–23, Feb. 2021.

[3] A. Hanson, "Opportunities in magnetic materials for high-frequency power conversion," *MRS Commun.*, vol. 12, no. 5, pp. 521–530, Aug. 2022.

[4] P. Ohodnicki. *Emergence of WBG Based Power Electronics and System Level Needs/Opportunities for Advances in Passives, Packaging, and Peripherals With Emphasis on HF Magnetics*. Accessed: Aug. 2020. [Online]. Available: https://www.energy.gov/sites/prod/files/2016/06/f32/06%20-%20OE%20ORNL%20Materials%20Innovation%20Workshop%20-%20Ohodnicki%20-%20small.pdf

[5] *2023 IEEE International MagNet Challenge, 2023 MagNet Challenge Handbook*. Accessed: Mar. 2023. [Online]. Available: https://github.com/minjiechen/magnetchallenge/blob/main/docs/handbook.pdf

[6] *Ansys Maxwell User's Manual V11*. Accessed: Sep. 2017. [Online]. Available: http://ansoft-maxwell.narod.ru/en/CompleteMaxwell3D_V11.pdf

[7] S. D. Sudhoff, *Power Magnetic Devices: A Multi-Objective Design Approach*. Hoboken, NJ, USA: Wiley, 2014.

[8] TDK. (Feb. 2023). *Ferrites and Accessories: SIFERRIT Material N87 Datasheet*. [Online]. Available: https://www.tdk-electronics.tdk.com/download/528882/990c299b916e9f3eb7e44ad563b7f0b9/pdf-n87.pdf

[9] J. Muhlethaler et al., "Core losses under the DC bias condition based on Steinmetz parameters," *IEEE Trans. Power Electron.*, vol. 27, no. 2, pp. 953–963, Feb. 2012.

[10] M. Mu et al., "New core loss measurement method for high-frequency magnetic materials," *IEEE Trans. Power Electron.*, vol. 29, no. 8, pp. 4374–4381, Aug. 2014.

[11] J. Muhlethaler et al., "Improved core-loss calculation for magnetic components employed in power electronic systems," *IEEE Trans. Power Electron.*, vol. 27, no. 2, pp. 964–973, Feb. 2012.

[12] D. C. Jiles and D. L. Atherton, "Theory of ferromagnetic hysteresis," *J. Magn. Magn. Mater.*, vol. 61, nos. 1–2, pp. 48–60, Sep. 1986.

[13] I. D. Mayergoyz, "Dynamic Preisach models of hysteresis," *IEEE Trans. Magn.*, vol. 24, no. 6, pp. 2925–2927, Nov. 1988.

[14] H. Li et al., "MagNet: A machine learning framework for magnetic core loss modeling," in *Proc. IEEE 21st Workshop Control Modeling Power Electron. (COMPEL)*, Nov. 2020, pp. 1–8.

[15] T. Guillod, P. Papamanolis, and J. W. Kolar, "Artificial neural network (ANN) based fast and accurate inductor modeling and design," *IEEE Open J. Power Electron.*, vol. 1, pp. 284–299, 2020.

[16] J. M. D. Coey, *Magnetism and Magnetic Materials*. Cambridge, U.K.: Cambridge Univ. Press, 2016.

[17] H. Cui, Z. Yao, and Y. E. Wang, "Coupling electromagnetic waves to spin waves: A physics-based nonlinear circuit model for frequency-selective limiters," *IEEE Trans. Microw. Theory Techn.*, vol. 67, no. 8, pp. 3221–3229, Aug. 2019.

[18] Q. Gao et al., "Demystify RF magnetics with linear and nonlinear equivalent circuit models," *IEEE Microw. Mag.*, vol. 23, no. 11, pp. 28–47, Nov. 2022.

[19] H. Tanaka, K. Nakamura, and O. Ichinokura, "Calculation of iron loss in soft ferromagnetic materials using magnetic circuit model taking magnetic hysteresis into consideration," *J. Magn. Soc. Jpn.*, vol. 39, no. 2, pp. 65–70, 2015.

PEM